

AD-A084 178 DREXEL UNIV PHILADELPHIA PA DEPT OF MATERIALS ENGINEERING F/6 11/4
MECHANISMS OF FAILURE IN METAL MATRIX COMPOSITES, (U)
1978 A PATNAIK, H ROGERS, M J KOZAK N00014-78-C-0130

UNCLASSIFIED

NL

1 of 1
AS
AD8-78

END
DATE
FILMED
6-80
DTIC

ADA084178

LEVEL 4

22

6 ANNUAL REPORT
MECHANISMS OF FAILURE
IN
METAL MATRIX COMPOSITES

By

A. Pattnaik
H. C. Rogers and M. J. Koczak

Drexel University
Department of Materials Engineering
Philadelphia, Pennsylvania 19104

11 1978

22

To

Naval Research Laboratory
Washington, D. C. 20375

15 N00014-78-C-0130

Approved for public release;
distribution unlimited

80 5 9 088

COMPRESSIVE FAILURE BEHAVIOR OF
FP ALUMINA/ALUMINUM COMPOSITES

A. Pattnaik, M. J. Koczak and H. C. Rogers
Department of Materials Engineering
Drexel University
Philadelphia, PA 19104

Failure of FP alumina/aluminum composite cylinders in axial compression has been investigated from the following points of view: (1) failure initiation, (2) post-failure deformation that usually accompanies compressive failure, and (3) strength as determined by specimen - and die-configurations. Correlation of microstructure with compressive strength values has been carried out qualitatively. Proper specimen and die configurations - necessary to prevent premature brooming failure - lead to transverse stress concentration regions, which in turn lead to localized, premature kinking failure.

Accession For

NTIS O.A&I	<input checked="" type="checkbox"/>
DCC TAB	<input type="checkbox"/>
Unannounced Notification	<input type="checkbox"/>

By *W. J. Koczak*

DATE *10/1/71*

1.

A

Introduction

Deformation and failure modes of composite materials under axial compressive load are quite complex and have been reviewed extensively (1-4). There is no single mechanism of failure that applies to all composite materials. The type varies depending on: (i) fiber type (ductile or brittle), (ii) matrix (ductile or brittle), and (iii) the interfacial bond strength, which controls delamination of fiber from the matrix under load. Compressive failure has been studied more extensively in brittle epoxy matrix composites than in ductile metal matrix composites (2,3). However, not all observations made with the epoxy matrix composites can be extended directly to metal matrix composites.

Three primary modes of failure have been observed: (i) splitting and lateral spreading of the fibers at the specimen ends called "brooming", which frequently occurs when flat dies are used, (ii) microbuckling (i.e., buckling of fibers against an elastic foundation), which can be of two types, namely, "extension mode" or "shear mode" depending on volume fraction of the fibers (5,6), and (iii) kinking, which entails microbuckling in the form of a "kink band" in a rather localized area of the composite. Local microbuckling that leads to kink band formation requires secondary shear stresses in addition to the primary compressive stress (7-10).

Even for homogeneous materials many complexities are involved in compression testing (11,12). These complexities are compounded during compression testing of composite materials; no standard procedure has yet been adopted by the research community.* The compressive failure stress and failure modes of composite materials appear to be more sensitive to the testing procedure than are homogeneous brittle materials. For example, brooming failure when flat dies are used occurs at relatively low stresses. The compressive strength increases if brooming is prevented either by using confining dies (14), by proper specimen design, or by applying confining hydrostatic pressure (9). Therefore, the existence of a "true" compressive failure strength is open to question. Greszczuk (4,15,16) for example, distinguishes between "microbuckling failure" and "ultimate compression failure". Generally the highest value of failure stress of those measured in any investigation is accepted as ultimate compression failure stress.

Preliminary results from the various experimental observations made on the compressive failure modes of FP alumina/aluminum fiber composites are discussed in the present paper. Particular attention has been directed to die and specimen configurations. Special techniques have been used in some instances to stop the post-failure deformation that usually accompanies compression testing, and the subsequent observations are discussed with respect to existing theoretical models. A detailed analysis of the results of the completed and ongoing tests will be presented at a later date (17).

Experimental Procedure

FP Alumina/Aluminum Composites

The composite was obtained from the manufacturer** in the form of rods 4.76 mm (3/16") or 9.52 mm (3/8") in diameter and plates (12 mm x 12 mm x 150 mm). These composites are made by a vacuum liquid infiltration technique (14). In the present investigation, the cylindrical specimens

* A standard procedure has been recommended by the ASTM for flat specimens (13).

** E. I. duPont de Nemours and Co., Wilmington, Delaware.

were centerless ground to 4.76 mm diameter; specimens of other configurations were machined with carbide tools followed by surface polishing using a flexible emery cloth.

Cylindrical specimens of various length to diameter (l/d) ratios at 35%, 45% and 55% fiber volume fractions (V_f) were tested; most of the testing reported here was carried out on specimens with $V_f = 55\%$. The diameter of the gage section was chosen to be 4.76 mm, based on the capacity of the Instron testing machine used.

Specimen and Die Configuration

Initially, cylindrical specimens were compressed between flat platens of 4340 steel heat treated to a hardness of $R_c = 55$. The composite failed by brooming at a stress level of 1,300 MPa (190 ksi), significantly lower than the 2,700 MPa (400 ksi) reported by Champion, et al (14).

Several alternative approaches to preventing premature brooming failure were examined. In one case, partially confining dies were used. They consisted of die blocks each of which contained a truncated conical hole. The diameter of the flat bottom was just that of the cylindrical specimens; the inclination of the die walls was from 5 to 15° to the cone axis. The small diameter base prevented brooming while the larger diameter conical walls were designed to restrict the lateral expansion that occurs at the local upset region to different degrees.

Two other types of specimen and die configuration were chosen for testing, Fig. 1. Both these configurations also prevented brooming failure. Detailed analyses of the composite failure mode were made on specimens from these two series. The specimen design shown in Fig. 1(a) with enlarged filleted heads was selected to permit easy specimen removal from the test fixture for prefailure measurement and examination of failure initiation sites. On the other hand the use of cylindrical specimens with "press-fit" steel collars compressed between flat dies (Fig. 1b) approximated the duPont grips but made removal for intermittent analysis difficult. This die-design, however, allowed the axial, post-failure deformation to be minimized by insertion of shims whose total thickness could be varied depending on specimen length.

When using the shims, a specimen was typically loaded to 80 to 90% of the expected ultimate failure stress, at which point the Instron cross-head movement was stopped. The gap between the two collars was measured by a thickness gage and shims of suitable thickness were inserted between them; testing was then continued to failure. With experience, the composite post-failure deformation could be nearly eliminated except for the effects arising from elastic deformation of the associated flat die or within the specimen itself. Without shims the permanent change in length (Δl) of a specimen after failure, was about 0.8 mm. By the use of shims, this change in length could be reduced to 0.08 mm without affecting the failure stress. By choosing shims of different thickness the post-failure deformation could be controlled within the range of 0.08 mm to 0.8 mm. The observed load drop during failure was also reduced as the change in length decreased.

The specimens were aligned between Instron machine platens by careful visual observation, aided by the cylindrical geometry of the specimen. All compression testing was carried out at a cross-head speed of 0.0003 cm/sec. The compression load cell used had a maximum load capacity of 89,000 N. At this load level, the Instron machine behaves like a soft machine (18) and the elastic unloading of the cross-head continues to squash the specimen after failure initiates.

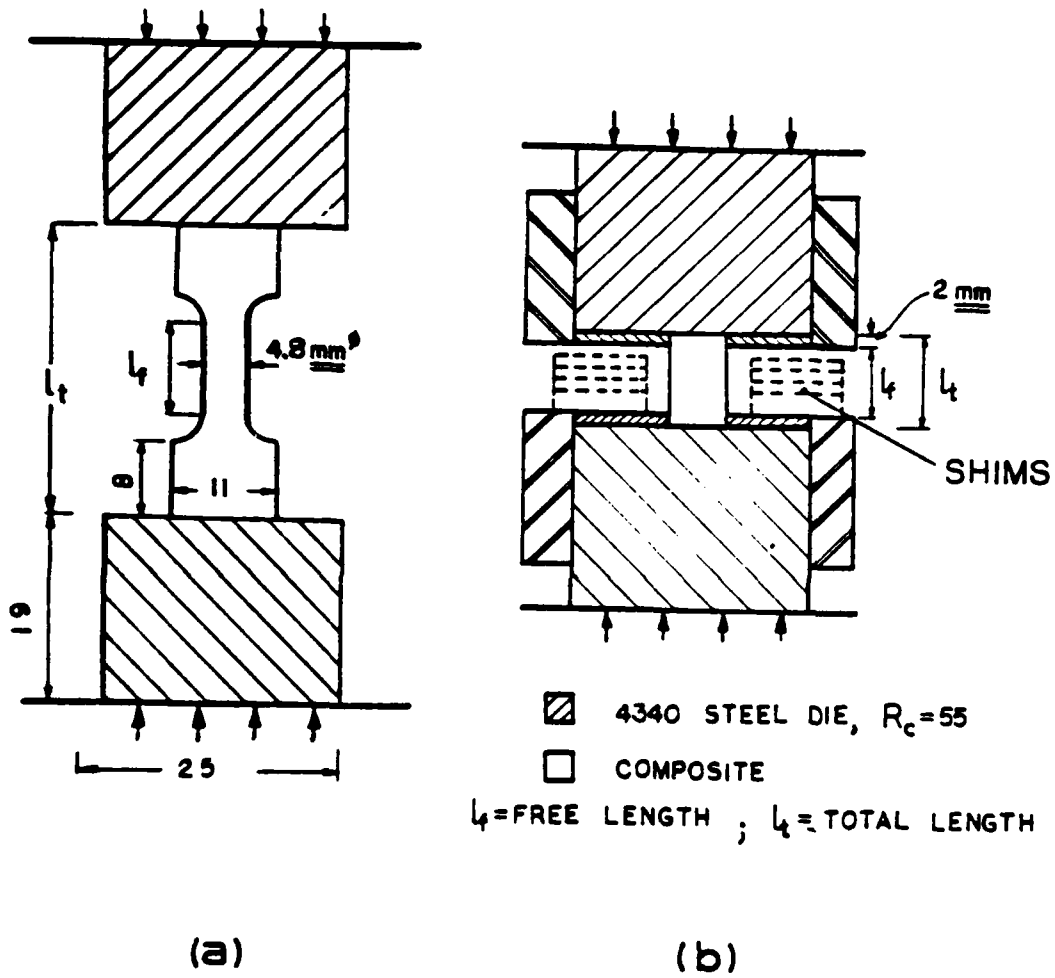


Figure 1. Two types of specimen and die configurations used in the present study.

Metallography

The specimens were cut with a liquid cooled diamond slitting wheel at a relatively low speed to avoid fiber cracking. After mounting the specimens in the standard manner, grinding was initiated on flat 320 grit emery paper. Low pressure was employed while grinding to prevent fiber breakage. Following 600 grit paper, the specimens were polished using 6 μ and 1 μ diamond paste on a flat Texmet* polishing cloth. A "figure eight" movement was employed while polishing them on these cloths (19). Final polishing was carried out with Linde B alumina powder (0.05 μ) on a Microcloth.*

The unetched specimens were observed metallographically under partially polarized light; this provided the best contrast among matrix, fiber, diffusion-zone, and voids. Some of the specimens were examined after failure in the scanning electron microscope. The failure surface was coated with a thin layer of gold to minimize charging effects.

Experimental Results

Metallography of As-Received Composite:

Transverse and longitudinal sections of as-fabricated FP alumina/aluminum composites are shown in Figs. 2(a), 2(c) and 2(b), respectively. The composite is made by vacuum liquid infiltration of Al-3 wt % Li alloy with FP alumina yarns held in position in a mold. Each yarn contains 210 filaments (fibers) with diameters in the range of 20 \pm 5 μ . A typical distribution of fibers in the cast composite is shown in Fig. 2(a). Observation at low magnification shows that the identity of the original yarns is not completely lost, and filaments in one yarn can be identified from the other. For example, the three fibers at the bottom of Fig. 2(a) belong to one yarn and have not reacted with the matrix to form a diffusion-zone. On the other hand the filaments at the top of Fig. 2(a) exhibit a distinct diffusion-zone between matrix and filament. The composition of the diffusion-zone has been analyzed and determined to be primarily Li₂O-5Al₂O₃ (20).

The scanning electron micrograph of a polished section, Fig. 2(c), shows many interesting features. Several voids are seen; they have arisen from a lack of penetration of the liquid metal into some of the crevices. A physical separation between some fibers and the matrix can also be seen which can be attributed to solidification shrinkage.

A longitudinal section is shown in Fig. 2(b). This and similar micrographs show that fibers are frequently not parallel to the section surface. Thus they appear to go in or out of the polished section, i.e., the fibers in the as-cast composite have "built-in" curvatures. Prewo (20) observed that some FP fibers in a similar composite were kinked and as a result the individual fibers exhibit a bimodal distribution of strength. A possible kink in an FP fiber is seen in the top left fiber of Fig. 2(b). The effects of such microstructural defects on compressive failure stress will be discussed later.

When cylindrical specimens were compressed between flat dies, the failure was usually by brooming, characterized by lateral spreading with longitudinal splitting. A portion of a typical brooming failure is shown in Fig. 3(a). The maximum compressive strength of specimens that failed by brooming when flat dies were employed was about 1300 MPa as shown in Table I. The stress-strain curves are approximately linear until very high stresses

* Trade name, Buehler Ltd., Evanston, Illinois

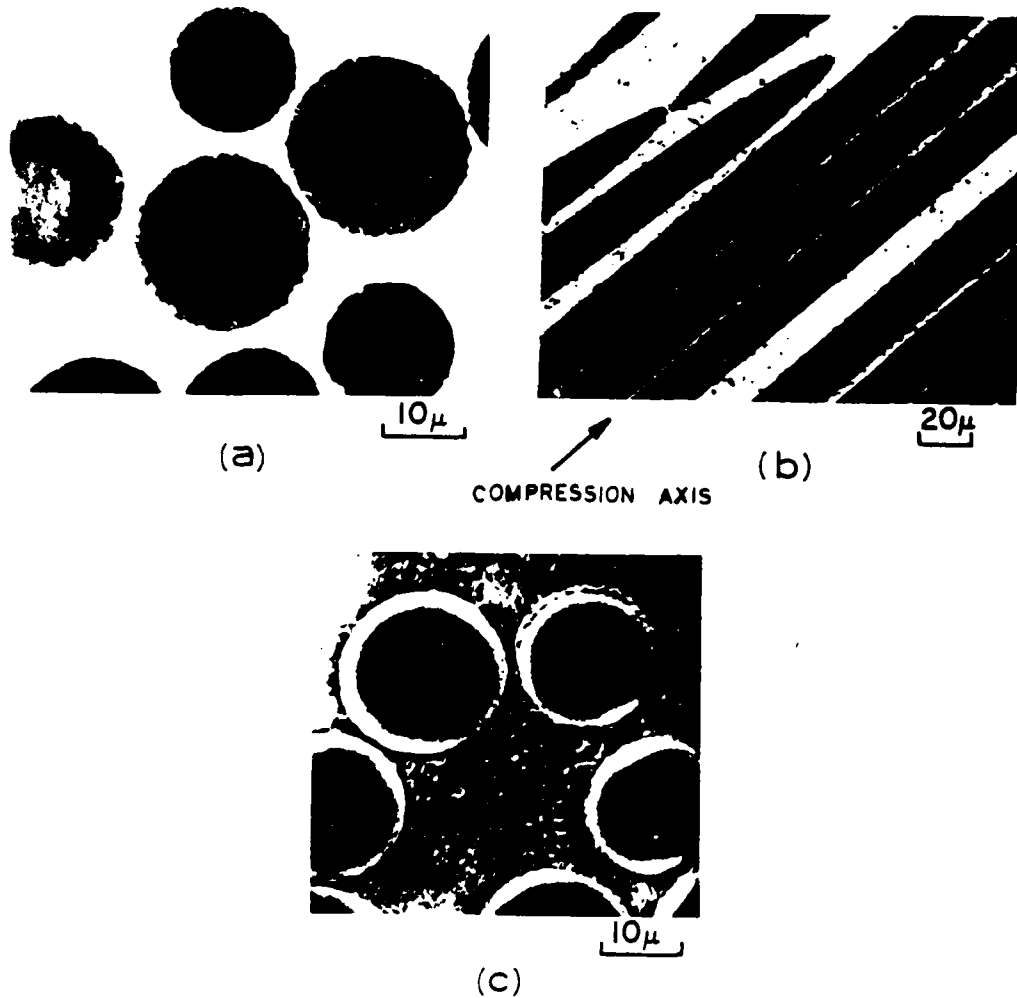
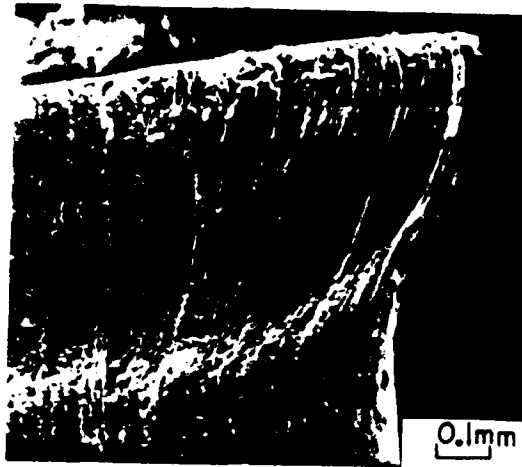
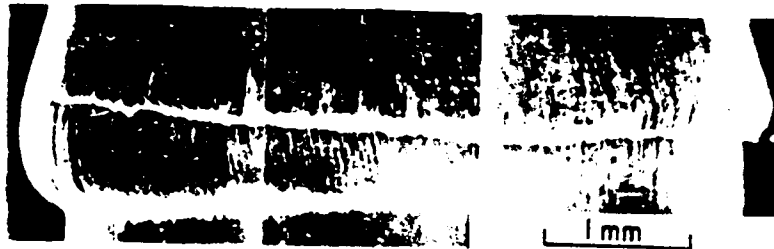


Figure 2. Microstructure of as-fabricated FP alumina/aluminum composite, $V_f = 55\%$. (a) Optical micrograph, bright field, 2000X; (b) Optical micrograph, bright field, 600X; (c) SEM micrograph, 2000X. (Reduced 40% for reproduction.)



FLAT DIES : BROOMING



CONFINING DIES, 15°

Figure 3. SEM micrographs of compression failure of FP alumina/aluminum composite. (a) Part of brooming failure; flat dies, $l/d = 1$, 100X. (b) Failure surface observed for dies with confining die-wall, 15°, $l/d = 3$, 50X. (Reduced 22% for reproduction.)

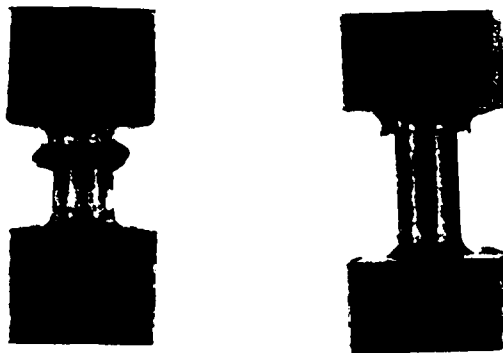


Figure 4. FP alumina/aluminum composite specimens after failure in compression. (a) $l/d = 1.32$, $r = 1.6$ mm, $\sigma_c = 2,840$ MPa; (b) $l/d = 2$, $r = 1.6$ mm, $\sigma_c = 2,770$ MPa.

Table I. Compressive Strength of FP Alumina/Aluminum

Composites, Cylindrical Specimens, $V_f = 55\%$ *

Flat Dies	Conical Constraining Dies	Filletted Specimens	Collar and Flat Dies
1,300 MPa (190 ksi)	1,600 MPa (240 ksi)	1,700-2,900 MPa (250-425 ksi)	2,400-3,000 MPa (350-430 ksi)

* A range of values were obtained because of variation in strengths due to different radius, (l/d) ratios, and die constraints.

are reached when they begin to develop a slight curvature. At upsetting there is a loud bang and a catastrophic drop in load the magnitude of which depends on the degree of upsetting. Brooming failure occurs at relatively low strength levels and hence, this failure mode can be considered to be "premature" failure.

Composite specimens with reduced gage sections and fillets, Fig. 1(a), exhibited high failure stresses (σ_C), failing in the manner shown in Fig. 4. The heads of these specimens acted as restraining dies to prevent brooming. Local upsetting failure always initiated near the point where the fillet radius ended and the straight portion began, i.e., at the point of maximum stress concentration, irrespective of radius size and (l/d) ratio. Specimens with larger (l/d) ratios exhibited somewhat different failure geometry, Fig. 4(b), compared with specimens with smaller (l/d) ratio, Fig. 4(a). Analysis of longitudinal sections of the failed specimens showed that the failure mechanism for the two specimens in Fig. 4 were essentially similar except the straight portion of the cylinder penetrated into the head for specimens with the larger (l/d) ratios, Fig. 4(b). This apparently results from the larger amount of elastic energy stored in the longer specimen being converted to increased plastic deformation. These shaped specimens, Fig. 1(a), gave rise to a range of σ_C values (depending primarily on the radius) of from 2,000 to 2,900 MPa (300-425 ksi). From Table I, a compressive strength of 2,800 MPa (400 ksi) is taken as the ultimate compressive strength of FP alumina/aluminum composite ($V_f = 55\%$) for comparison with theoretical models (see section on discussion).

Figures 5 and 6(a) show respectively the observed effect of fillet radius and gage length on the composite failure stress. Although there is some scatter at small fillet radii and the number of specimens tested is too small to develop a good statistical base, there appears to be a clear trend toward reduced maximum compressive strength, σ_C , with increasing fillet radius. This unexpected result will be discussed in the next section. The trend toward increasing strength with increasing length up to a maximum as seen in Fig. 6(a) also appears to be clear cut.

The failure surface of an FP alumina/aluminum composite cylinder, which has been compressed using conical constraining dies (15° die-wall), is shown in Fig. 3(b). The SEM micrograph shows the external evidence of a kinking failure in the composite. Brooming as such has been suppressed but the upsetting has taken place near the end. Furthermore, as seen in the micrograph the lateral growth of an individual upset (kink or microband) region has been terminated early by the restraining die wall. The elastic unloading of the specimen and testing machine has continued by means of the formation of multiple intersecting bands giving rise to a particularly complex geometry. This has been confirmed by metallographic observation of a longitudinal

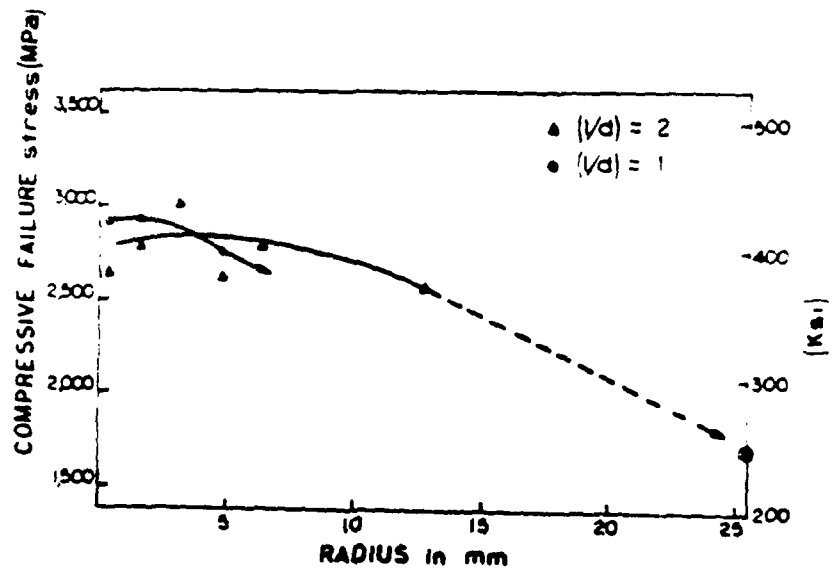


Figure 5. Variation of ultimate compressive strength of FP alumina/aluminum composite with radius, specific to the specimen configuration shown in Fig. 1(a).

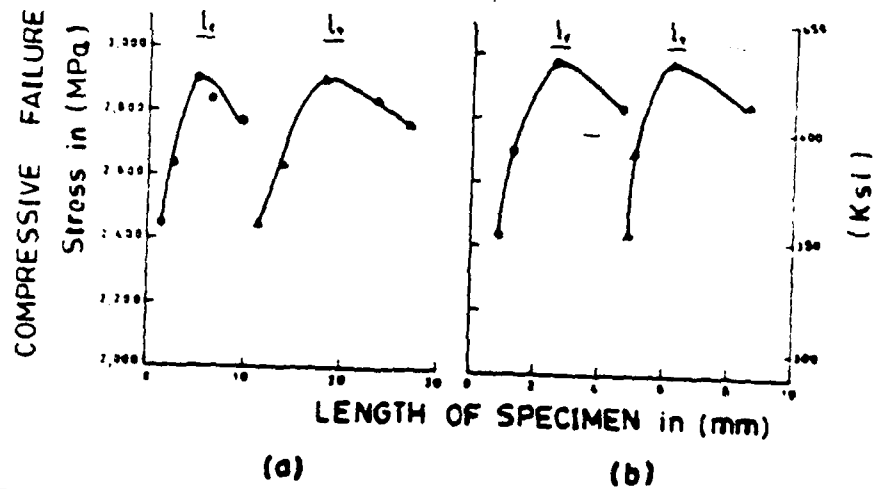


Figure 6. Variation of ultimate compressive strength with the length of specimen; All data refer to $l/d \leq 3$. (a) refers to filleted specimens shown in Fig. 1(a) and (b) refers to the specimens shown in Fig. 1(b).

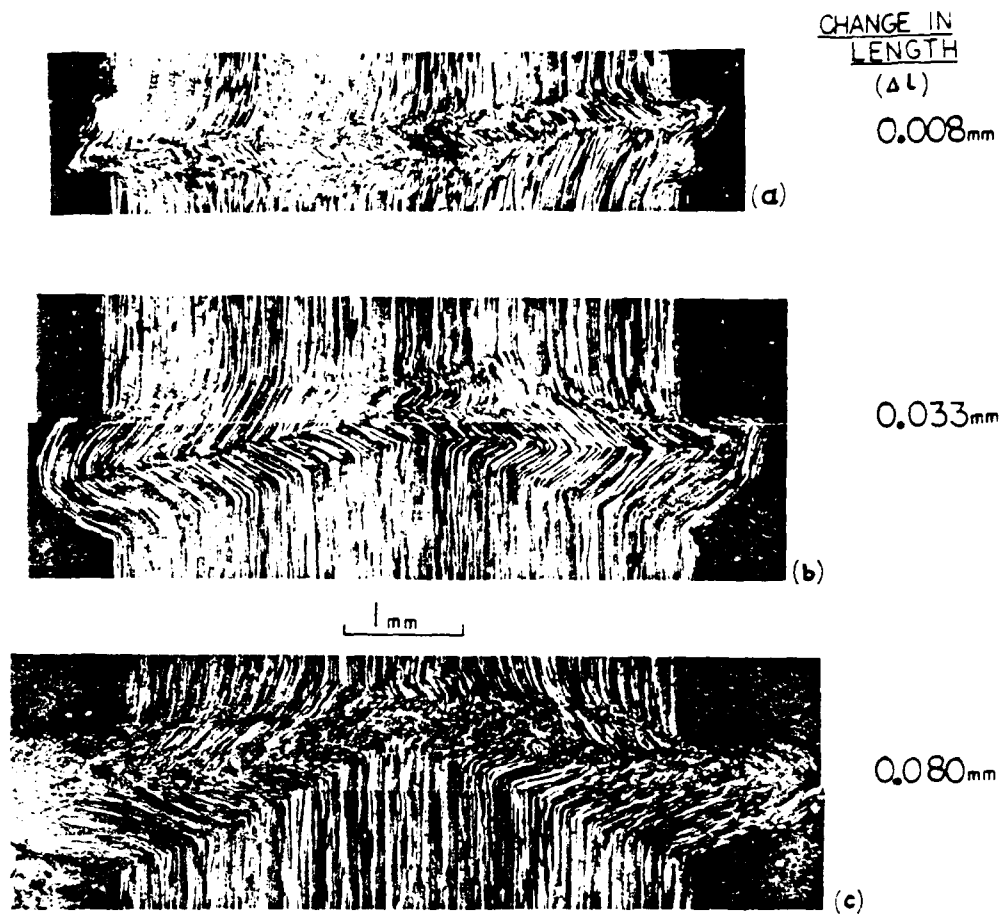
section through the upset region. A similar type of compression failure has been observed in a shock-loaded single crystal by Klassen-Neklyudova et al. (21). Failure occurred by the rocking from side to side of the crystal as a result of the alternate motion of conjugate kink bands. Because of this complexity the use of the flat dies, collars, and shimming was considered a more likely approach to stopping the failures at different stages in their development.

Subsequently, then, compression testing was carried out on cylindrical specimens with dies as shown in Fig. 1(b). The "press-fit" collars (height 2 mm) were successful in preventing brooming failure but apparently also acted as stress concentrators because failure again initiated at one end right above the collar. The height of the collars was kept to a minimum so that short specimens could be compressed to failure. The advantage of this compression fixture was that the post-failure deformation could be reduced to a minimum, or controlled to a desired level, by the insertion of shims during an interrupted compression testing.

From the limited data on this type of specimen, the σ_C also decreased with decreasing specimen length (either the "free length" or the total length, Fig. 1(b)), Fig. 6(b). Unfortunately, after failure the specimens were always jammed into the collar rings and had to be forced out, frequently resulting in fracture. Longitudinal sections of cylindrical composite rods failed in this set up are shown in Fig. 7. The structure of the failed region of an unshimmed composite is shown in Fig. 7(c). Similar structures were observed in the upset region of failed filleted specimens as seen in Fig. 4. The structure shows evidence of some form of kinking but post-failure deformation has further forced the fibers outward leading to a more complex structure. Further clarification of the mechanism of formation of such a structure was obtained when the post-failure deformation was reduced in a controlled manner by the use of shims and shorter specimens. However, using shorter specimens led to a decrease in the ultimate compressive strength σ_C , as shown in Fig. 6(b). This agrees with the observations using filleted specimens, Fig. 6(a), but is contrary to a previous observation (15) at least in the increasing portion of the curve in which the mechanism of failure of model laminated composites was microbuckling. The reason for such behavior lies with the mode of failure and stress concentration, which will be elaborated upon in the discussion.

Discussion

What became abundantly clear after testing many specimens of this material is that their behavior is rather complex and it is difficult to translate the results of studies of homogeneous, isotropic materials to the behavior of these heterogeneous, strongly anisotropic materials. For example, in the specimens with a reduced gage section rather than a gradual stress transfer from the small gage section to the larger heads as the fillet cross section increases, the specimens under load actually behave, in part, more like cylinders having the diameter of the gage section surrounded at either end by restraining collars of varying cross-section and thickness made of the composite material itself. This is clear from several observations. First, the initially flat ends of filleted specimens that engage the hardened steel platens take on a configuration in which the central circular portion, of radius equal to that of the gage section, is found after testing to be raised relative to the remainder of the end surface of the head. This is most probably the result of this central cylindrical column of composite bearing nearly the entire load and thus elastically indenting the platen (no residual platen indentation could be observed). Plastic deformation of the aluminum matrix in the composite allows the end surface to permanently conform to the elastically indented platen. Another



FP Al_2O_3 /ALUMINUM COMPOSITE FAILURE
IN COMPRESSION $V_f = 55\%$

Figure 7. Optical micrographs of longitudinal sections of FP alumina/aluminum composite cylinders, which have failed in compression using collar dies shown in Fig. 1(b). Increasing amount of post-failure deformation is observed from (a) to (c).

possibility is that the highly loaded central column expands laterally from Poisson's expansion, thus expanding the ring-like remainder of the head. Constancy of volume could cause the ring to contract axially as it is expanded. This is relatively unlikely, however, because the high strength of the composite in the direction of the fibers would minimize axial contraction in favor of reducing the radial thickness of the "restraining collar" since the lateral strength of the composite is in the neighborhood of 1/8 to 1/10 of their axial strength (14). Furthermore, the lateral bulge that results from upsetting failure is located at the start of the fillet at one of the ends and therefore is normally quite close to the head. Because of the nature of the bulge, the region of outward extrusion of fractured material often penetrates the fillet or head region. Because of the low transverse strength of the composite a form of "petalling" can take place, Fig. 4(b), when the restraining fillet ring is cracked and forced outward. In severe cases, particularly when the height of the head was reduced, the entire head is split radially accompanied by tangential separation or partial separation from the central composite cylinder.

Finally, when the height of the heads were reduced further, the ends of the central cylinder broomed, the outer composite ring not being sufficiently strong to prevent brooming. In this case also, there was splitting and separation of the outer head material from the central core.

Failure Mode:

The normal mode of compression failure in these FP alumina/aluminum composite appears to be a type of kinking or multiple kinking. The formation of kink bands is shown schematically in Fig. 8. Failure by formation of a simple kink, Fig. 8(a), has been reported in boron-polyimid, epoxy composites (8), glass-reinforced plastics (25), and in hot-pressed tungsten-2024 Al composite laminates (26). In the present investigation conjugate kinks with intersections have generally been observed, Figs. 7(a) and 7(b). The first simple kink is intersected by another simple kink at approximately equal angles forming a conjugate kink with intersection, shown schematically in Fig. 8(b). The direction of rotation of the fibers in the second simple kink is opposite to that of the first kink and hence tends to realign the two ends of the specimen, Fig. 8(a). The specimen in Fig. 7(a) underwent a change in length of only 0.008 mm. It is quite conceivable that only a simple kink would form if the post-failure deformation could be reduced to zero (17).

When the collar dies were used, the kinks always initiated near the collars, resulting in the flat portion seen in Fig. 7. As the upset material is extended outward it is constrained axially on one side by the flat collar. It is not obvious whether each simple kink initiated at a local surface region and then propagated across the cylinder or a diffuse kink formed, then intensified. The second kink is not as well developed as the first kink in Fig. 7(a). It is clear from Fig. 7(b), however, that a kink band generally extends from one side of the specimen to the other side.

The general conformation of the upset bulge region is approximately the same for specimens having heads with generous fillet radii and the cylinders compressed with the ends restrained by collars. The purpose of the fillets is to minimize stress concentration at the head-gage section interface. The normal and shear stresses due to circular openings and steps have been analyzed as stress concentrators for homogeneous (22,23) and also for composite materials (24). The decrease in σ_c with increasing radius is difficult to explain by the variation in stress concentration with increase in radius alone. Although the situation is far from completely clear, it is

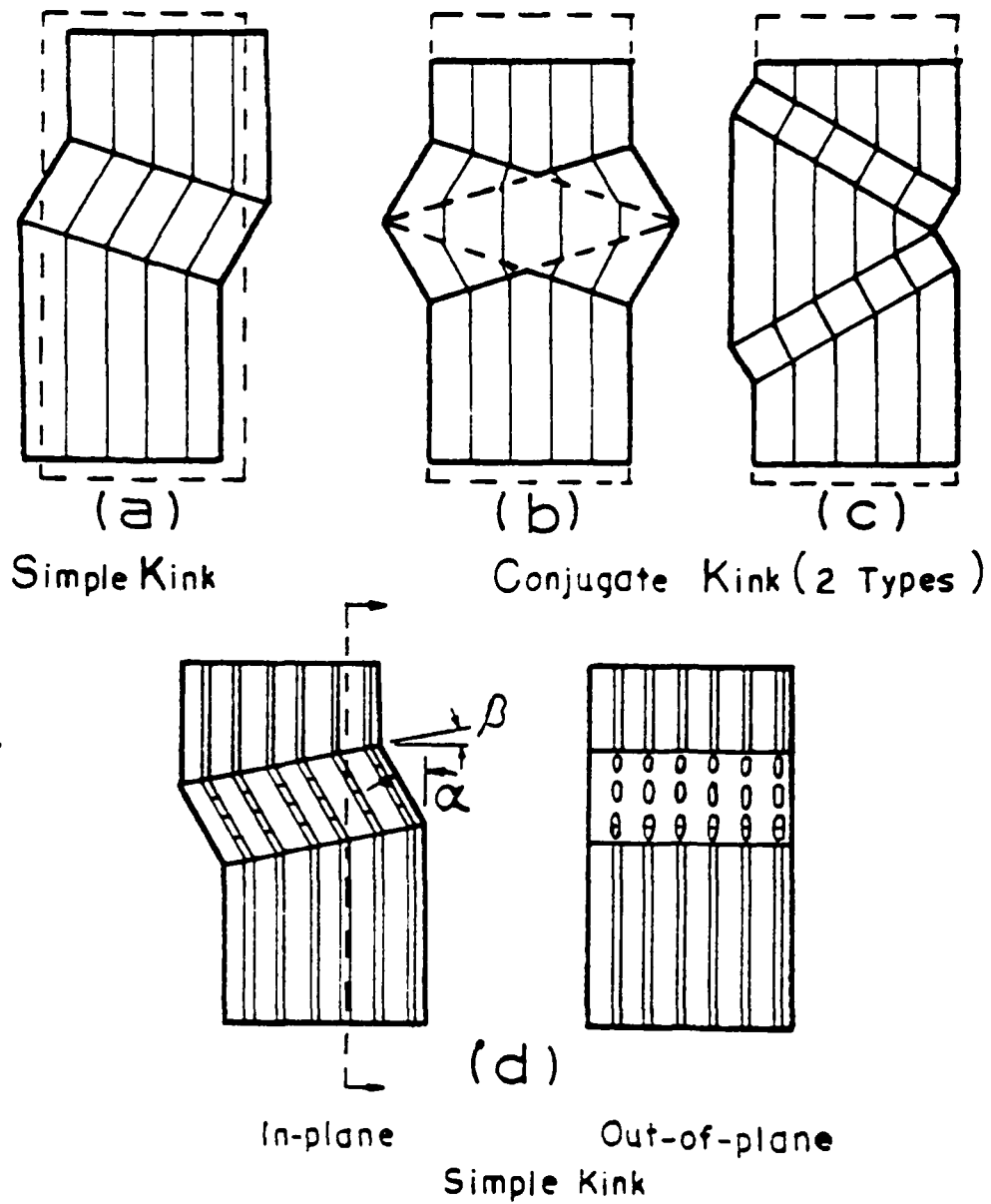


Figure 8. Schematics describing simple and conjugate kinks, (a), (b) and (c); the in-plane and out-of-plane kink morphologies are shown in (d). The kink inclination (α) and boundary orientation (β) are also indicated.

felt that this apparent anomaly results from the two competing effects of a decreasing fillet radius: increased axial stress concentration while simultaneously generating increasing lateral supporting stresses and supporting material bulk that tend to suppress lateral fiber buckling.

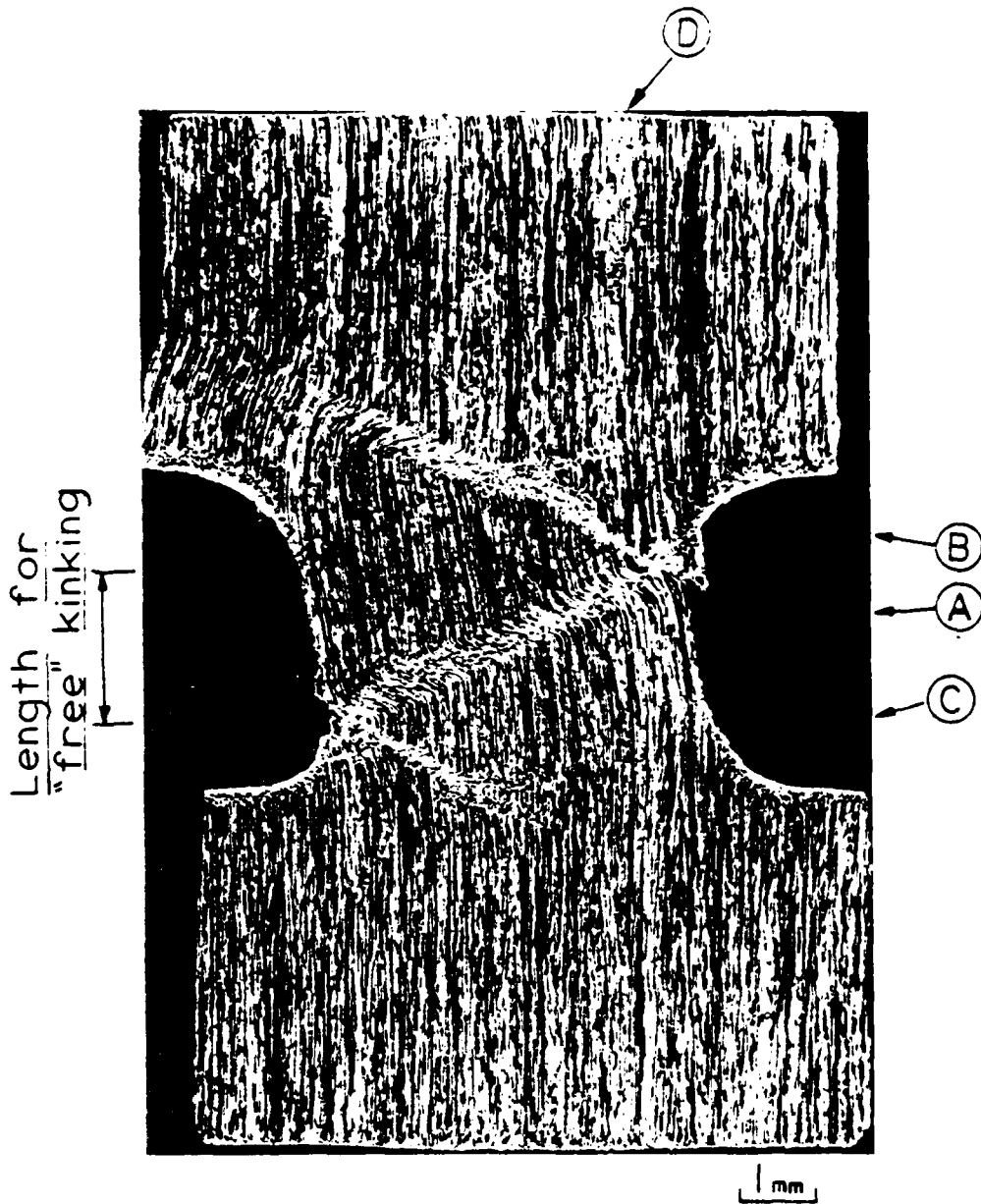
Chaplin (25) has studied the initiation and propagation of a kink band originating at a notch in glass-reinforced plastics. Evidence of initiation and propagation of a simple kink at the point of stress concentration is observed in the composite shown in Fig. 9. This specimen was a short specimen (gage length = 2.4 mm) with a fillet radius of 1.6 mm. It should be noted that the volume fraction of fiber was only 45% in this case, although this is probably not significant to the arguments about kinking. The kinks (A) and (B) in Fig. 9 clearly indicate that non-intersecting conjugate kinks, shown schematically in Fig. 8(c) are initiated at the root of the fillet radius and propagate along an inclined plane that forms the kink boundaries, Fig. 8(d). A third simple kink (C) can either independently originate at a point of stress concentration as part of a second pair of non-intersecting conjugate kinks, or can originate from the kink already formed (A) when it intersects the lower fillet as seen in Fig. 9. The second process is dictated from geometry considerations as it tends to reduce possible bending stresses and realign the two ends of the specimen. Some displacement is still observed between the two ends of the specimen in Fig. 9, however.

Both in-plane and out-of-plane simple kinks, Fig. 8(d), are observed in the present axisymmetric composite specimens, Figs. 7 and 9. The direction of tilt for the formation of a kink has been extensively studied by Orringer (2), who concluded that buckling patterns that precede kink formation, Fig. 9, are always planar. Moreover, he found that direction of buckling lay along the direction of minimum fiber spacing, which he attributed to a matrix failure. It is not clear that this conclusion is applicable here. The kink patterns observed in Fig. 9 were not usually observed, the typical ones being shown in Fig. 7. As seen in Fig. 9 (point D) a band of pure matrix existed in this sample, possibly contributing to the formation of conjugate kinks without intersection. Whatever differences in detail may exist, the specimen shown in Fig. 9 strongly suggests kinking as the mode of compression failure in FP alumina/aluminum composites.

The structure of a simple kink is seen in greater detail in Fig. 10(a). The structure of a kink band in the propagation stage is shown in Fig. 10(b). A kink band which has undergone post failure deformation has greater fiber degradation, Fig. 10(c). The fibers have broken into a series of short lengths of remarkably consistent periodicity, the fracture initiating on the tension side of the bent fibers apparently at a critical tensile strain. Similar observations have been made on carbon-epoxy composites (9); the periodicity of fiber cracking was explained by the limiting surface strain with the buckled lengths breaking in half as postulated by Berg and Salama (8).

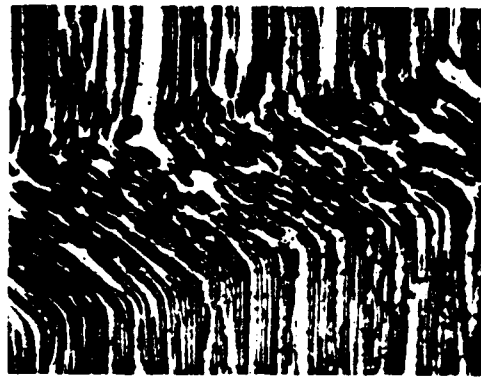
Unlike carbon-epoxy composites (9), very few voids or delamination were observed in the present composite. Because the matrix in the present study is a ductile aluminum alloy, the voids created by fiber cracking are filled by metal flow under the high compressive stresses. This type of kink band with fibers broken at fixed intervals within the band, was not observed in carbon-carbon composites by Evans and Adler (10).

Is microbuckling a precursor to the formation of a kink band, seen in Figs. 9 and 10? This question cannot be answered from the observation of the micrographs in Figs. 9 and 10. It is possible that a stress field is set up ahead of a propagating kink band, which leads to microbuckling of fibers ahead of the kink band. This seems to be a plausible assumption from strength considerations. Similarly, it can be postulated that local microbuckling initiates near a point of stress concentration, leading to the



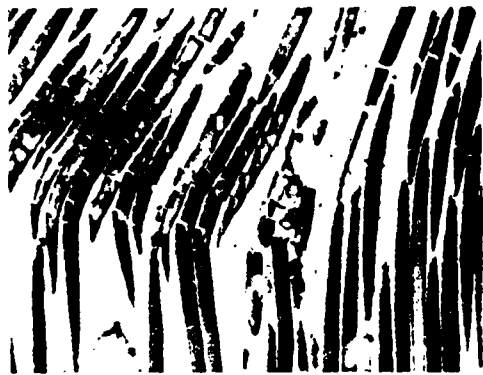
Conjugate Kink without
intersection

Figure 9. Longitudinal section of FP alumina/aluminum composite, failed in compression. $V_f = 45\%$, $l/d = 0.5$, $r = 1.6$ mm, $\sigma_c = 2,350$ MPa.



(a)

400 μ



(b)

200 μ



(c)

50 μ

Figure 10. Structure of kink bands in FP alumina/aluminum composite. Partially polarized light, optical micrographs; (a) 50X, (b) 200X, and (c) 500X. (Reduced 40% for reproduction).

formation of a kink band, which then propagates outwards on an inclined plane. The geometry of a kink band is shown in Fig. 8(d). The kink inclination (α) and the kink boundary orientation (β) define the geometry of a kink band. Evans and Adler (10) observed a range of values for α and β , with upper and lower bounds for both of them. Their analysis of 'shear kinking' leads to a predicted $\alpha = 67^\circ$, which was considered to be in good agreement with experimental observation. We believe, however, that the range of values of α and β arises from post-failure deformation of a kink band, as seen in Figs. 7 and 11. Future theoretical analysis should aim at explaining the angles of α and β when post-failure deformation is zero (17).

Ultimate Compressive Strength

Theoretical calculations of the axial, compressive strength have been put forward and they have been reviewed in the literature (1-4). For practical composites, i.e., $V_f > 20\%$, the ultimate compressive strength (σ_C) for failure by 'shear mode' or 'in-phase' microbuckling is given by (5):

$$\sigma_C = \frac{G_m}{1 - V_f} \quad (1)$$

Where σ_C = ultimate compressive stress

G_m = matrix shear modulus

V_f = volume fraction of fibers (55%)

Equation (1) was derived for elastic buckling of fibers against an elastic foundation; a two-dimensional laminate model was assumed for theoretical analysis. The shear modulus of Al - 4 wt % Li alloy is 30,340 MPa (4.4×10^6 psi) (27), which gives $\sigma_C = 67,500$ MPa (9800 ksi). This value is more than 20 times the experimental value of 2,800 MPa (400 ksi). This is not surprising since the mode of failure in FP alumina/aluminum composite is kinking rather than microbuckling.

If microbuckling of fibers occurs against a plastic foundation (i.e., m x plastically deforming) the equation of inelastic buckling is given by (8):

$$\sigma_C = \left[\frac{V_f \cdot E_f \cdot \sigma_{ym}}{3(1-V_f)} \right]^{1/2} \quad (2)$$

where E_f = Young's modulus of fibers

σ_{ym} = matrix yield stress.

In the present composite, $E_f = 345$ GPa (50×10^6 psi) (taking the lower limit) and $\sigma_{ym} = 193$ MPa (28 ksi) (27), giving $\sigma_C = 5,200$ MPa (755 ksi). This calculated strength value is still nearly twice the experimentally measured value.

Greszczuk (16) recently has derived an equation for shear mode microbuckling of a circular composite (3-dimensional model):

$$\sigma_C = G_{LT} + \pi^2 \cdot E_f \cdot V_f \cdot (r/l)^2 \quad (3)$$

where $G_{LT} = G_{12}$ = shear modulus of the composite

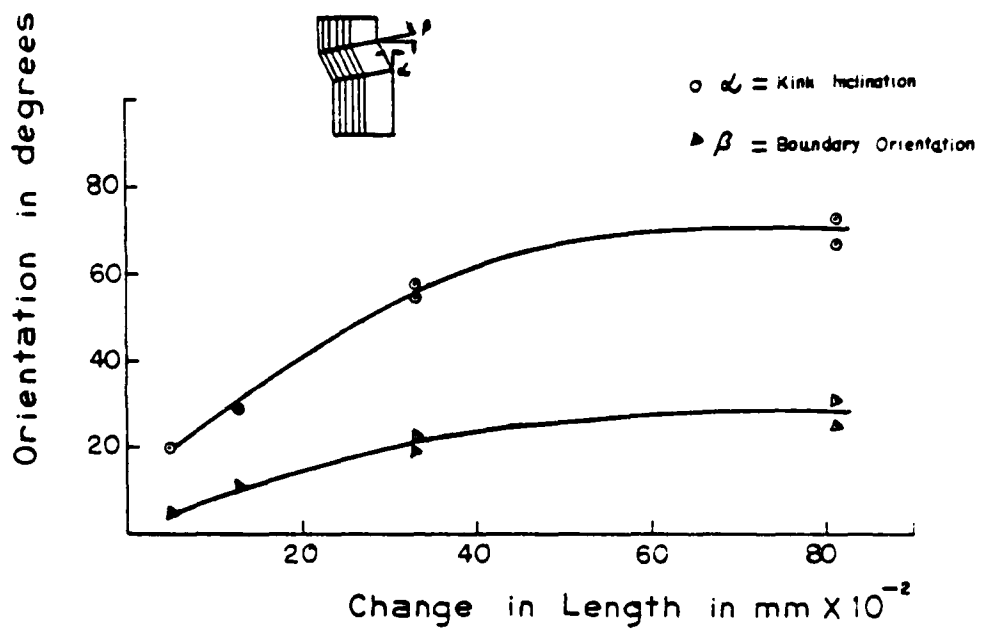


Figure 11. Kink orientation relationship as a function of post-failure deformation (Δl). Δl = initial length - length after failure.

r = fiber radius

l = buckle wavelength or specimen length

For small values of (r/l) , as is the case in the present study where $r = 20 \pm 5\mu$, Equation 3 can be written as

$$\sigma_C = G_{LT} \quad (4)$$

The shear modulus of the present composite ($V_f = 55\%$) is approximately 49 GPa (7.1×10^6 psi) (14). This gives a very high value for σ_C , even higher than that given by Equation (1).

Argon (29) derived a simple equation for failure stress in compression based on shear instability leading to kinking failure, which gave

$$\sigma_C = \frac{\sigma_{ym}}{2\theta_0} \quad (5)$$

where σ_{ym} = matrix yield stress

θ_0 = initial misalignment of the fibers

However, the misalignment, θ_0 , is a qualitative term. Moreover, stress concentration effects could reduce the σ_C to values lower than that given by Equation (5). In the present composite, stress concentrations as well as fiber misalignment exists (Figs. 1 and 2) thereby making strength calculations difficult. Not only is it difficult to quantify the fiber misalignment, θ_0 , in the present composite, but the stress concentration factor is also unknown and variable, Figs. 1, 5, 6.

In summary, the experimentally measured values for ultimate compressive strength of FP alumina/aluminum composites fall far short of theoretical predictions. However, an understanding of the failure mode has clarified the reasons for the low strength values. Local stress concentration leads to local inelastic microbuckling of brittle alumina fibers which break, thus leading to kink band formation (9,10). Theoretical calculations σ_C under such conditions are quite complex. In order to achieve higher compressive strengths than that determined in this investigation one has to eliminate stress concentrators in a compression specimen. This is not easy if brooming failure is to be prevented. Microstructural defects, like voids and the physical separation between the fiber and matrix, shown in Fig. 2, apparently are not the sites of failure initiation in this composite. Rather, the local upsetting begins at the surface, which is a site of both concentrated stress and of structural weakness with respect to matrix support for the fibers under compressive loading.

According to Equation (3) σ_C should increase with decreasing length of compression specimen, if the (r/l) is significant with respect to G_{LT} . However, σ_C decreases with decreasing specimen length in the present investigation, Fig. 6, over most of the range tested. This is not surprising as Equation (3) refers to microbuckling of the whole composite specimen (15,16), while kinking appears to be the mode of failure in the FP alumina/aluminum composites. In particular, kinking initiates at a stress concentrator, Fig. 9. As seen in this figure, the kink boundary orientation is inclined to the fiber axis. If the length of the

specimen is shorter than the length required for free kinking, the tendency for failure is enhanced because the stresses from the root of one radius can overlap those generated by the radius at the other end (23). This can lead to an increasing σ_c with increasing specimen length, Fig. 6. It is not clear at present why the failure stress should begin to decrease with length as the length gets large. Although it agrees in principle with trends demanded by Equation (3), the values of $r/2$ in this system are so small that the second term of Equation (3) should not be significant.

Conclusions

1. Kinking is the mode of compressive failure in FP alumina/aluminum composite cylinders. Kinking is probably initiated by local, inelastic microbuckling, which takes place at stress concentration points or at other local inhomogeneities.
2. Study of the controlled post-failure deformation following catastrophic compressive failure has thrown new light into the initiation of failure modes in this composite system.
3. Theoretical predictions of kink orientation and failure stress due to kinking should take the post-failure deformation into consideration.
4. Presence of voids, initial misalignment of fibers, and possible physical separation between the fiber and the matrix in the FP alumina/aluminum composite lead to experimental compressive strength values much lower than those predicted by the existing theories of compression failure.

Acknowledgment

The authors would like to thank Drs. R. Weimer and C. Sanday of the Naval Research Laboratory for their encouragement and interest in this program which was supported under Contract No. 00014-78-C-0130.

References

1. Jones, R. M.: Mechanics of Composite Materials, McGraw Hill Publ., New York, 1975, p. 134.
2. Orringer, O.: AFOSR Scientific Report, ASRL TR162-1 (AD-734789), October 1971, p. 9.
3. Corten, H. T.: Modern Composite Materials, Broutman, L. J. and Krock, R. H., eds., Addison-Wesley Publ., 1967, p. 97.
4. Greszczuk, L. G.: Analysis of the Test Methods for High Modulus Fibers and Composites, American Society for Testing of Matls., ASTM STP 521, 1973, p. 192.
5. Rosen, B. W.: Fiber Composite Materials, American Society for Metals Publ., 1965, p. 37.
6. Kulkarni, S. V., Rice, J. S. and Rosen, B. W.: Composites, vol. 6, 1975, p. 217.

THIS PAGE IS BEST QUALITY PRACTICABLE
FROM COPY FURNISHED TO DDC

THIS PAGE IS
FROM COPY FURNISHED TO DDC

7. Patterson, M. S. and Weiss, L. E.: Geolog. Soc. of America Bull., vol. 77, 1966, p. 343.
8. Berg, C. A. and Salama, M.: J. of Matls., JMLSA, vol. 7, No. 2, 1972, p. 216.
9. Weaver, C. W. and Williams, J. G.: J. of Matl. Science, vol. 10, 1975, p. 1323.
10. Evans, A. G. and Adler, W. F.: Acta Met., vol. 25, 1978, p. 725.
11. Kuhn, H. A. and Dieter, G. E.: Fracture 1977, ICF4, Waterloo, Canada, vol. 1, 1977, p. 307.
12. Kendall, K.: Proc. Roy. Soc., London, vol. A361, 1978, p. 245.
13. Standard Method for Test for Compressive Properties of Oriented Fiber Composites, 1978 Annual Book of ASTM Standards, Part 36, 1978, p. 853.
14. Champion, A. R., Krueger, W. H., Hartman, H. S. and Dhingra, A. K.: Paper presented at the Second Internat. Conf. on Composite Materials, Toronto, Canada, April 16-20, 1978.
15. Greszczuk, L. B.: Composite Materials: Testing and Design (Third Conf.), ASTM STP 546, American Soc. for Testing of Matls., 1974, p. 5.
16. Greszczuk, L. B.: AIAA Journal, vol. 13, No. 10, 1975, p. 1311.
17. Pattnaik, A., Koczak, M. J. and Rogers, H.: To be published.
18. McGregor, Tegart, W. J.: Elements of Mechanical Metallurgy, The Macmillan Co. Publ., New York, 1966, p. 25.
19. Bertone, T. J.: Metallographic Specimen Preparation - Optical and Electron Microscopy, McCall, J. L. and Mueller, W. M., eds., Plenum Press Publ., New York, 1974, p. 251.
20. Prewo, K. M.: Report R77-912245-3, United Tech. Research Center, East Hartford, Conn., May 1977.
21. Klassen-Neklyudova, M. V., Chernysheva, M. A. and Tomilovskii, G. E.: Soviet Physics-Crystall., vol. 5, 1961, p. 617.
22. Knott, J. F.: Fundamentals of Fracture Mechanics, John Wiley, 1976, p. 29.
23. Marsch, D. M.: Fracture of Solids, Drucker, D. C. and Gilman, J. J., eds., John Wiley, New York, 1963, p. 119.
24. Greszczuk, L. B.: Composite Materials: Testing and Design (Second Conference), American Soc. for Testing of Matls., ASTM STP 497, 1972, p. 363.
25. Chaplin, C. R.: J. of Matls. Science, vol. 12, 1977, p. 347.
26. Ruzauskas, E. J.: M.S. Thesis, Drexel University, June 1972, p. 37.
27. Santner, J. S.: Report TM-LL-75-13, Air Force Materials Lab., Wright-Patterson Air Force Base, Ohio, August 1975, p. 9.
28. Down, F., Rosen, B. W. and Hashin, Z.: NASA-CR-492, June 1966.

29. Argon, A. S.: Treatise on Materials Science and Technology, Academic Press, vol. 1, 1972, p. 79.